Nanotechnology

Thin Dielectric Layer Enabled Low Voltage Operation of Fully Printed Flexible Carbon Nanotube Thin Film Transistors

Thin Dielectric Layer Enabled Low Voltage Operation of Fully Printed Flexible Carbon Nanotube Thin Film Transistors

Jialuo Chen [1], Saswat Mishra [2], Diego Vaca [2], Nitish Kumar [2], Woon-Hong Yeo [2,3], Suresh Sitaraman[2], and Satish Kumar [2]

[1] School of Electrical and Computer Engineering, Georgia Institute of Technology, Atlanta 30332, USA
[2] G. W. Woodruff School of Mechanical Engineering, Georgia Institute of Technology, Atlanta 30332, USA
[3] Wallace H. Coulter Department of Biomedical Engineering and Petit Institute for Bioengineering & Bioscience, Georgia Institute of Technology, Atlanta 30332, USA

Corresponding author: jlchen@gatech.edu, satish.kumar@me.gatech.edu

ABSTRACT

Quality of printable dielectric layer has become one of the major obstacles to achieve high performance fully printed transistors. A thick dielectric layer will require high gate voltage to switch on and off the transistors, which will cause high power dissipation in printed devices. In response to this challenge, fully printed carbon nanotube (CNT) based thin film transistors (TFTs) have been fabricated on flexible membranes such as polyimide and liquid crystal polymer using aerosol jet printing (AJP). These devices can be operated at bias voltages below ±10 V (drain/gate voltages around ±6 V). It is much smaller than the previously reported values for fully printed CNT-TFTs using xdi-dcs (mixture of poly(vinylphenol)/poly (methylsilsesquioxane)) as dielectric and using a single printing method. This is enabled because of thin dielectric layer (~300 nm) and good uniformity in printed CNT network. The printed CNT-TFTs show on/off ratio > 10^5, and mobility > 5 $cm^2V^{-1}s^{-1}$. Layer-by-layer deposition of CNT allows highly uniform and dense network formation, and the optimization of the xdi-dcs concentration using natural butyl alcohol provides a high-yield printing of a thin dielectric layer. Collectively, this work shows a potential of using fully printed CNT-TFTs in various flexible electronic applications such as wearable sensors, actuators, artificial skins, displays and wireless tags and antennas.

KEYWORDS: *fully printed thin film transistors, printed dielectric, xdi-dcs, carbon nanotube network, flexible electronics, aerosol jet printing*

1. Introduction

Printed electronics on flexible substrates has attracted significant attention in recent years because of the high potential in wearable and bendable devices [1]. Its applications include flexible displays [2], radiofrequency identification (RFID) antennae/tags [3, 4], sensors [5, 6], artificial skins [7], etc. Among various printing techniques, aerosol jet printing (AJP) has been proven to be capable of printing microelectronic devices and relevant circuits with low-cost, repeatability, scalability, and relatively high precision compared with other printing techniques [8, 9]. AJP has been utilized to deposit a wide range of materials because it can handle inks viscosities in the range of 1-1000 Cp [10]. The superior electrical, mechanical, and chemical properties of single-walled carbon nanotubes (CNTs) make them very promising as the channel material in thin film transistors (TFTs) [11, 12]. As a one-dimensional nanoscale material, CNTs has exceptional high current carrying capacity [13, 14]. Extraordinary flexibility [15-17] and elasticity [18] can also be expected when CNTs undergoes high strain and bending, which is also the key advantage of using CNT for flexible devices. Printed CNT-TFTs with improved carrier mobility, device stability, variability, and dissipation power have significant potential for many applications [19-23].

Even though the advances in printing techniques, synthesis and processing of nanomaterials have brought fresh impetus to the development of printed flexible devices [24], the tradeoff between cost and performance still limits their applications. Fully printed CNT-TFTs are crucial for low-cost fabrication because lithography steps and deposition techniques such as atomic layer deposition (ALD) typically used for gate-dielectric synthesis will complicate the process and increase the cost at the same time. On the other hand, high performance is hard to achieve for fully printed CNT-TFTs. The causes are different, such as imperfections in the electrode patterns, contact quality at the interfaces, uniformity of the CNT network, thickness of the dielectric layer, etc. [25]. Most of them need to be addressed properly, e.g., nanoparticle silver (Ag) inks [26] for contacts, highly purified semiconducting CNT inks [27] for TFT-channel; and ion-gels, barium titanate ($BaTiO_3$), xdi-dcs, etc. as dielectric inks [28-30] [31]. Here, xdi-dcs is a blend of poly(vinylphenol)/poly(methyl silsesquioxane) (PVP/pMSSQ).

In previous studies, flexible CNT-TFTs were fabricated using different printing techniques, including inkjet printing (IJP) [19, 32, 33], AJP [8, 10, 34], screen printing [35], roll-to-roll gravure [5, 36, 37], as well as some combination of printing systems [36]. For fully printed CNT-TFTs, one of the primary obstacles to enable low voltage operation lies in printing a good quality gate-dielectric layer because of the lack of high-quality printable inks. One of the most straightforward solutions to address this is to use ALD for the dielectric deposition. Kim et al. fabricated CNT-TFTs using a combination of IJP and ALD [33], e.g., electrodes, semiconductors, and vias, were realized by IJP, but Al_2O_3 was deposited using ALD as dielectric layer, which resulted in ambipolar transistors and circuits with high operational stability. Like Kim, most of the previous work used nonprinting methods to pattern dielectrics or some other elements of TFTs during fabrication. Homenick et al. demonstrated fully printed CNT-TFTs using an integrated roll-to-roll gravure/IJP system (not a single printing system) [36], which yielded good CNT network uniformity in fully printed TFTs on liquid crystal polymers (LCP) substrates. Cai et al. also reported fully printed CNT-TFTs using hybrid gate dielectric comprising PDMS and $BaTiO_3$ nanoparticles [30]. Cao et al. pointed out the disadvantages of $BaTiO_3$/PMMA as the gate dielectric, which highly depends on the size, shape, and spatial distribution of nanoparticles [31]. In their work, a thick hydrophobic layer using xdi-dcs was printed as gate dielectric (~2µm, to avoid pin holes) of CNT-TFTs on Kapton substrate leading to negligible hysteresis. However, this thick dielectric layer severely limited their performance, and achieving thin printed dielectric without pin holes is still very challenging. Cao et al. investigated methods to improve the electric contacts in fully printed CNT-TFTs by employing different printed contact materials and contact geometries [20]. Andrew et al. introduced eutectic gallium−indium liquid metal contacts for printed CNT-TFTs to achieve stretchable transistors. [24]. Cardenas et al. fabricated CNT-TFTs using a low-temperature and entirely in-place AJP approach without removal of the substrate from the printer. Low contact resistance to semiconducting CNTs were achieved without the use of high-temperature baking steps [38]. However, the high threshold voltage in these TFTs highly limited their performance because the gate bias has to be as large as ±40V to fully switch on/off the transistors. Ion gel could be an alternative solution to address the specific problem of high threshold voltage [28, 29, 39], but ion gel based printed CNT-TFTs exhibit ambipolar performance with high leakage and static power consumption [31]. It is fragile compared to other dielectric materials.

In this work, fully printed CNT-TFTs were fabricated on both Kapton and LCP substrates utilizing only AJP technique. For comparison, some other CNT-TFTs (non-fully printed) were also fabricated whose dielectric were grown by ALD. The performance of fully printed devices was significantly improved by optimization of the printed xdi-dcs layer, which can be a superior gate dielectric material for printed devices because it avoids the issues reported in the previous studies by other researchers when using BaTiO3/PMMA [30] (particle-like printing) and ion gel [40] (stability, environment sensitive). The CNT network was printed as the channel material of TFTs using a solution of single-walled CNTs in toluene, whose concentration was 0.01 mg/ml. More than 99% of the CNTs in the solution were semiconducting. A highly uniform CNT network film was achieved by performing a layer-by-layer deposition method, which largely decreases the CNT bundling effect and provides an effective way for the density control. Printing of single conductive layer of CNT network improved the on/off ratio of the fully printed devices. The printing of xdi-dcs thin film as gate dielectric was realized by diluting and optimizing the ink with natural ≥99.5% butyl alcohol in appropriate wt-%, and applying plasma treatment for better surface wetting. The fabricated CNT-TFTs showed very stable performance with on/off current ratio as high as ~10^5, mobility with average value of 4.9 $cm^2V^{-1}s^{-1}$, low hysteresis with average value of 0.6 V, and good uniformity of the CNT network. More importantly, these TFTs can be operated under gate voltages below ±10V. For the first time, those CNT-TFTs are fabricated with a printed xdi-dcs layer as thin as ~300nm, free of pin-holes, leading to low voltage operation. This work achieved lower operating voltage (±6V) for fully printed flexible devices using xdi-dcs as dielectric based on a single printing method. This improvement is key for the application of CNT-TFTs based circuits in printed electronics on flexible substrates because of the lower voltage operation and power dissipation.

2. Experimental

The fabrication process of the fully printed CNT-TFTs is shown in Figure 1. Kapton (DuPont, USA) with thickness of 127µm (±10%) and LCP films (Rogers, USA) with thickness of 150-200µm, were used as the flexible substrates. They were rinsed by acetone, isopropyl alcohol (IPA), and deionized (DI) water successively, then blown dry by N_2 gun. Next, 5min oxygen plasma (100W) was applied for better surface preparation, which is followed by Ag printing (Ag ink: UTD Ag Conductive Silver Nanoinks, UT Dot) as source and drain (S/D) electrodes using Optomec aerosol jet printing system AJ200. Then Ag patterns are sintered at 150°C for 15~25min in an oven. Before CNT printing (CNT ink: IsoSol-S100® Polymer-Wrapped Nanotubes, NanoIntegris), 30s oxygen plasma was applied to functionalize the surface which could help achieve uniformly distributed CNT network. A thorough cleaning of AJ200 would be indispensable when changing from Ag to CNT ink (2~3hours ultrasonic, then acetone, IPA, DI water, and toluene rinse successively). After CNT printing, toluene rinse was used to wash away the excess surfactant and polymers on the surface, followed by thermal annealing at 120°C for >1hour in the oven. After that, xdi-dcs thin layer was printed (with sheath gas flow rate of 40CCM and printing speed of 10mm/s as default settings) as gate dielectric (xdi-dcs ink: Xerox Research Center Canada), which was diluted and optimized with natural ≥99.5% butyl alcohol (Sigma Aldrich) in appropriate %, and cured by thermal annealing at 140°C for 20min in the oven. Then 2-3min oxygen plasma was applied to make the xdi-dcs surface hydrophilic again before Ag printing to fabricate gate electrodes on top, followed by Ag cure at 150°C for 15~25min. Ultrasonic atomizer is good enough for the printing of all inks involved. The smallest channel length achieved was ~20μm. The sheath gas flow rate, ultrasonic atomizer flow rate, and printing speed are chosen differently to control the printing quality with respect to different inks. The additional fabrication details can be found in supporting information (Figure S1-S4). Figure 2 describes the structure and scanning electron microscope (SEM) images of the printed CNT-TFTs. Figure 2(a) displays fully printed CNT-TFTs using xdi-dcs as gate dielectric.

3. Results and Discussion

For comparison, CNT-TFTs with ~80nm aluminum oxide (Al_2O_3) layer as gate dielectric were fabricated using ALD at 100°C, replacing the xdi-dcs layer for new CNT-TFTs (ALD based CNT-TFTs), depicted in Figure 2(c) (the rest fabrication steps are the same). CNT network is printed on top of S/D electrodes, which is shown to have better contact than S/D on top of CNT network[20]. Top gate is used in the CNT-TFTs to achieve lower hysteresis (Figure S5 of supporting information) of the devices, as CNT network is not in direct contact with the environment. The morphology of the CNT-TFTs (as-printed Ag, CNT network, and xdi-dcs) on flexible substrates can be seen in

Figure 2(b). CNT network is only visible by using SEM. Figure 2(b)-middle shows uniform CNT network resulting from layer-by-layer deposition method, i.e., CNT printing, toluene rinsing, and blown dry processes (1 cycle altogether) are performed repeatedly for density control and to acquire highly uniform CNT network (normally 2~4 cycles). The significance of oxygen plasma treatment and layer-by-layer deposition on CNT network uniformity can be observed in Figure 3. Without oxygen plasma, CNTs tend to bundle together because of the hydrophobic nature of the surface, thus the corresponding network is non-uniform and it is hard to control the density. After the treatment, density control can be achieved through layer-by-layer deposition, which is more efficient than density control by using different concentration of CNT solution. Similar improvement is also achieved for Ag printing on top of xdi-dcs thin film.

The performance of fully printed CNT-TFTs is mainly limited by the gate dielectric. The printing of a xdi-dcs thin film is critical to obtain relatively high-performance CNT-TFTs. During AJP printing, the thickness of xdi-dcs can vary in large range based on the dilute ratio of xdi-dcs as well as the printing parameters such as sheath gas flow rate (SG), ultrasonic atomizer flow rate (UA), and printing speed (PS). For a given SG/US/PS combination, the thickness variation (as shown in Figure S4) can result from various factors such as the stability and accuracy of the AJP printer, the surface quality of substrate or previously printed features, the curing process of the dielectric layer, etc. All these factors should be considered, while attempting to reduce dielectric thickness (330 ± 140 nm), to avoid the failure of dielectric layer during device fabrication. The thinnest xdi-dcs film we achieved for a CNT-TFT is ~0.3μm (SG=18CCM and PS=10mm/s as default setting unless stated otherwise, UA=30CCM in this case), and the thickest is close to 1μm (measured by Tencor P15 profilometer). Figure 4 displays the difference in transfer characteristics caused by the thickness of xdi-dcs thin film. The difference in thickness is controlled by the values of UA, which are 30CCM, 32CCM, and 36CCM for 0.33μm, 0.41μm, and 0.59μm respectively. Except for the values of UA, the fabrication process and other parameters/dimension are exactly the same for the CNT-TFTs (W=500μm, L=100μm, 2-cycle CNT network deposition). Figure 4(a) compares the transfer curves of fully printed CNT-TFTs with different thickness of dielectric layers. It is clear that the range of V_g needed to fully switch on and off the devices depends on the thickness of printed xdi-dcs layer. As observed from the figure, for the device with thickness of 0.33μm, V_g has to be swept between -8V ~ 6V in order to reach on/off ratio of 10^5. However, V_g has to be swept in the range of -10V ~ 16V in order to switch on and off the device with thickness of 0.59μm. Obviously, the thicker the printed dielectric layer, the larger V_g is needed for the transistor to operate at its highest on/off ratio. This is because the gate capacitance is directly related with the thickness of dielectric, which affects the transconductance of the transistors. Figure 4(b) plots the dependence between the thickness of printed xdi-dcs layer and V_{th} for a set of fully printed CNT-TFTs (each cross denotes a different CNT-TFT). These CNT-TFTs were fabricated using exactly the same process and parameters except that the PS value is different in order to control the thickness of the xdi-dcs layers. Generally, a positive correlation can be seen from the plot, i.e., if the printed dielectric layer is thicker, the transistor tends to have higher value of V_{th}. However, it is very difficult to obtain a one-to-one relationship between the thickness of printed xdi-dcs layer and V_{th} because V_{th} also depends on other factors such as operation temperature, charges in dielectrics, etc. (which is hard to control for state of art printed CNT-TFTs even though they are fabricated exactly the same way). The xdi-dcs thin film with thickness less than 0.3μm can easily cause short between gate and S/D electrodes, while an overprinting can appear with ink spill outside the designed feature when the thickness is larger than 1μm, which should be avoided. Table 1 compares the performance (both hysteresis and operation voltage V_g) of some printed

CNT-TFTs in literature, which were fabricated using different printing methods. It is clear that ion-gel based devices have better performance compared to the rest, but printed ion-gel is very fragile. ALD based devices [33] are not fully printed, which will increase the fabrication cost. The performance of polymer based ([41] – [36], [36] uses combination of printing methods for fabrication) devices varies largely depending on the fabrication method and dielectric material used. Compared to other polymer based devices, especially considering fully printed CNT-TFTs, the devices in this work have obvious advantage of low operation voltages because of the improvement in xdi-dcs based dielectric layer. And the improvement in the uniformity of CNT network results in very high on/off ratio of the fully printed devices.

Even though thin xdi-dcs layer is the key for fully printed CNT-TFTs, it is difficult to print films thinner than 0.3μm because the pinholes in such thin films (<0.3μm) can easily cause short circuit TFT (~ pinhole effect, which fails to provide insulation between gate and S/D electrodes). Figure 5(a) illustrates the structure we used to test the insulation quality of printed xdi-dcs thin film, which is similar to the structure in fully printed CNT-TFTs. Undoubtedly, good insulation (leakage current << 0.1nA) of printed dielectric is the precondition for fully printed CNT-TFTs. The measured capacitance of printed xdi-dcs thin film is in range of 6 to 8 nF/cm^2 with thickness changing from 0.8 to 0.3 μm, respectively. Generally, the poor quality of xdi-dcs layer results from the severe pinhole effect when current can flow directly from the gate electrode (red electrode in Figure 5(a)) to the S/D electrodes (~black electrode in Figure 5(a)). To optimize the quality of printed xdi-dcs layer, natural ≥99.5% butyl alcohol is used to dilute the xdi-dcs ink with a dilution ratio σ (defined as volumetric ratio of xdi-dcs : butyl alcohol) ranging from 1:1 to 1:4. Figure 5(b) shows the printed xdi-dcs layers at different σ and UA, which are the two key parameters for controlling quality of printed xdi-dcs thin film. As shown in this figure, when σ is 1:1

corresponding to low dilution, continuous thin layer can't be formed. Instead, the printed features show particle-like morphology with numerous small pinholes. When σ is 1:4, the morphology of printed features is highly uneven with several large pinholes (red dash area in Figure 5(b)). When UA is as large as 35CCM, over spill of the ink from the nozzle will ruin the substrate (over printing). Clearly, over printing of xdi-dcs can cause additional problems too. In general, good morphology of printed features can be achieved when σ is around 1:2.5, which results in very uniform and continuous xdi-dcs thin film and the thickness can be well controlled by changing UA accordingly.

Based on the structure displayed in Figure 5(a), 5 samples are fabricated for each combination of σ and UA, with σ varying from 1:1 to 1:4 and UA varying from 22CCM to 42CCM. Numerator/denominator format is used to describe the results. When denominator equals 5, it denotes the result is for a specific σ and a specific UA. When denominator equals 30, it denotes the result is for a specific σ and all UA. The yield counts the number of samples without short between the red Ag electrode and the two black Ag electrodes sandwiched with printed xdi-dcs thin film. The results can be seen in Figure 6(a). The yield rate of samples with good insulation quality are 0/30, 2/30, 4/30, 16/30, 12/30, 2/30, 0/30 (denominator is the number of all samples; numerator is the number of good samples) when σ equals to 1:1, 1:1.5, 1:2, 1:2.5, 1:3, 1:3.5, 1:4 respectively with UA changing from 22 to 42CCM for each σ. Similarly, those values are 0/30, 0/30, 7/30, 13/30, 11/30, 5/30 when UA equals to 22, 26, 30, 34, 38, 42CCM respectively with σ changing from 1:1 to 1:4 for each UA. Therefore, (σ, UA)=(1:2.5, 34), would be one of the best combinations for the printing of xdi-dcs thin film. Other combinations such as (σ, UA)=(1:2.5, 38) and (σ, UA)=(1:3, 34) are also very reliable in the test. The value of σ is more important because it cannot be adjusted freely during printing, and should be determined before printing. Figure 6(b) plots the thickness dependence on UA of printed xdi-dcs thin film when σ is determined as 1:2.5

in advance. UA can be changed freely as needed during printing. To guarantee the stability of the ink mist of xdi-dcs, the printing is performed 2min after the changing of UA value. The time interval for each printing cycle (1^{st} cycle, 2^{nd} cycle, and 3^{rd} cycle) is roughly 1 hour. Generally, the dependence in Figure 6(b) should be linear because of mass conservation. However, the printing becomes unstable when UA>40CCM (σ=1:2.5). Over printing can happen when UA is close to 50CCM, which is similar as depicted in Figure 5(b) when (σ, UA)=(1:4, 35). The data inside the black dash box of Figure 6(b) corresponds to high yield rate which can be observed in Figure 6(a). Collectively, the thinnest xdi-dcs film is around 0.3μm in fully printed CNT-TFTs. By optimizing the printing process without shortage of electrodes, it can enable on and off switching using V_g below ±10V.

The I–V characteristics of the CNT-TFTs was measured using the Microtech Summit 11 k probe station and Keithley 4200 SCS. We fabricated a series of devices with the same channel width (W=500μm), but different channel lengths (L=50~250μm). The output characteristics (I_d-V_{ds} curves) and the transfer characteristics (I_d-V_{gs} curves) of the CNT-TFTs are plotted in Figure 7. Figure 7(a) and 7(b) are ALD based CNT-TFTs, Figure 7(c) and 7(d) are fully printed CNT-TFTs. The on/off ratio of the fully printed CNT-TFTs ranges from 10^3 to 10^6, which increases with increasing channel length because of lower probability for metallic CNTs to form conductive path. The random CNT network can also cause difference in on/off ratio. The overall I–V characteristics shows p-type performance with mobility ranging from 2 to 8 $cm^2V^{-1}s^{-1}$.

4. Conclusions

Fully printed CNT-TFTs have been fabricated on flexible substrates using AJP. The fabricated devices can be fully switched on and off using V_g below ±10V to reach on/off ratio as high as ~10^5. Single layer and multiple layers of CNT network are printed and analyzed, which facilitates density control as well as highly uniform CNT network structure. By diluting xdi-dcs with natural (≥99.5%) butyl alcohol in appropriate volumetric ratio (σ=1:2.5), printed dielectric thin film with thickness of ~0.3μm is achieved in fully printed CNT-TFTs. A high quality printed dielectric layer free of the pinhole effect is demonstrated with high yield rate by controlling the UA value. The achieved improvement in the printed dielectric layer is crucial for lower voltage operation of flexible transistors and lower power dissipation, which paves the path for employment of CNT-TFTs as building blocks in flexible wearable devices such as high-performance displays, radiofrequency identification tags, sensors, artificial skins, etc.

Supplementary Material: Supplementary material is available (fabrication details of CNT-TFTs using aerosol jet printing: the aerosol jet 200 system, printing parameters of Ag/CNTs/xdi-dcs, schematic of fully printed CNT-TFTs, statistics of mobility and on/off ratio of fully printed CNT-TFTs, measured heights of printed layers of CNT-TFTs, and hysteresis of printed CNT-TFTs).

References

[1] C. Wang *et al.*, "Extremely bendable, high-performance integrated circuits using semiconducting carbon nanotube networks for digital, analog, and radio-frequency applications," *Nano letters,* vol. 12, no. 3, pp. 1527-1533, 2012.

[2] L. Cai *et al.*, "Direct printing for additive patterning of silver nanowires for stretchable sensor and display applications," *Advanced Materials Technologies,* vol. 3, no. 2, p. 1700232, 2018.

[3] J. Zhang, G. Y. Tian, A. M. Marindra, A. I. Sunny, and A. B. Zhao, "A review of passive RFID tag antenna-based sensors and systems for structural health monitoring applications," *Sensors,* vol. 17, no. 2, p. 265, 2017.

[4] R. Singh, E. Singh, and H. S. Nalwa, "Inkjet printed nanomaterial based flexible radio frequency identification (RFID) tag sensors for the internet of nano things," *RSC Advances,* vol. 7, no. 77, pp. 48597-48630, 2017.

[5] M. Bariya *et al.*, "Roll-to-Roll Gravure Printed Electrochemical Sensors for Wearable and Medical Devices," *ACS nano,* 2018.

[6] J. Chen, A. Lotfi, P. J. Hesketh, and S. Kumar, "Carbon nanotube thin-film-transistors for gas identification," *Sensors and Actuators B: Chemical,* vol. 281, pp. 1080-1087, 2019.

[7] G. Yu, J. Hu, J. Tan, Y. Gao, Y. Lu, and F. Xuan, "A wearable pressure sensor based on ultra-violet/ozone microstructured carbon nanotube/polydimethylsiloxane arrays for electronic skins," *Nanotechnology,* vol. 29, no. 11, p. 115502, 2018.

[8] M. Ha *et al.*, "Aerosol jet printed, low voltage, electrolyte gated carbon nanotube ring oscillators with sub-5 μs stage delays," *Nano letters,* vol. 13, no. 3, pp. 954-960, 2013.

[9] G. Grau, J. Cen, H. Kang, R. Kitsomboonloha, W. J. Scheideler, and V. Subramanian, "Gravure-printed electronics: recent progress in tooling development, understanding of printing physics, and realization of printed devices," *Flexible and Printed Electronics,* vol. 1, no. 2, p. 023002, 2016.

[10] A. Mahajan, C. D. Frisbie, and L. F. Francis, "Optimization of aerosol jet printing for high-resolution, high-aspect ratio silver lines," *ACS applied materials & interfaces,* vol. 5, no. 11, pp. 4856-4864, 2013.

[11] J. Chen and S. Kumar, "Variability in Output Characteristics of Single-Walled Carbon Nanotube Thin-Film Transistors," *IEEE Transactions on Nanotechnology,* vol. 17, no. 2, pp. 353-361, 2018.

[12] M. Jeong, K. Lee, E. Choi, A. Kim, and S.-B. Lee, "Spray-coated carbon nanotube thin-film transistors with striped transport channels," *Nanotechnology,* vol. 23, no. 50, p. 505203, 2012.

[13] T. Dürkop, S. Getty, E. Cobas, and M. Fuhrer, "Extraordinary mobility in semiconducting carbon nanotubes," *Nano letters,* vol. 4, no. 1, pp. 35-39, 2004.

[14] S.-J. Choi, P. Bennett, D. Lee, and J. Bokor, "Highly uniform carbon nanotube nanomesh network transistors," *Nano Research,* vol. 8, no. 4, pp. 1320-1326, 2015.

[15] D. Lee *et al.*, "Logic circuits composed of flexible carbon nanotube thin-film transistor and ultra-thin polymer gate dielectric," *Scientific reports,* vol. 6, 2016.

[16] I.-C. Cheng, "Flexible and Printed Electronics," in *Materials for Advanced Packaging*: Springer, 2017, pp. 813-854.

[17] B. Tian *et al.*, "Carbon nanotube thin film transistors fabricated by an etching based manufacturing compatible process," *Nanoscale,* 2017.

[18] B. I. Yakobson, C. Brabec, and J. Bernholc, "Nanomechanics of carbon tubes: instabilities beyond linear response," *Physical review letters,* vol. 76, no. 14, p. 2511, 1996.

[19] P. M. Grubb, H. Subbaraman, S. Park, D. Akinwande, and R. T. Chen, "Inkjet printing of high performance transistors with micron order chemically set gaps," *Scientific reports,* vol. 7, no. 1, p. 1202, 2017.

[20] C. Cao, J. B. Andrews, A. Kumar, and A. D. Franklin, "Improving contact interfaces in fully printed carbon nanotube thin-film transistors," *ACS nano,* vol. 10, no. 5, pp. 5221-5229, 2016.

[21] Y. Che, H. Chen, H. Gui, J. Liu, B. Liu, and C. Zhou, "Review of carbon nanotube nanoelectronics and macroelectronics," *Semiconductor Science and Technology,* vol. 29, no. 7, p. 073001, 2014.

[22] Q. Cao and J. A. Rogers, "Random networks and aligned arrays of single-walled carbon nanotubes for electronic device applications," *Nano Research,* vol. 1, no. 4, pp. 259-272, 2008.

[23] N. Kumar, J. Chen, M. Kar, S. K. Sitaraman, S. Mukhopadhyay, and S. Kumar, "Multigated Carbon Nanotube Field Effect Transistors-Based Physically Unclonable Functions As Security Keys," *IEEE Internet of Things Journal,* vol. 6, no. 1, pp. 325-334, 2018.

[24] J. B. Andrews *et al.*, "Patterned Liquid Metal Contacts for Printed Carbon Nanotube Transistors," *ACS nano,* 2018.

[25] D. M. Sun, C. Liu, W. C. Ren, and H. M. Cheng, "A Review of Carbon Nanotube‐and Graphene‐Based Flexible Thin‐Film Transistors," *Small,* vol. 9, no. 8, pp. 1188-1205, 2013.

[26] K. R. Zope, D. Cormier, and S. A. Williams, "Reactive Silver Oxalate Ink Composition with Enhanced Curing Conditions for Flexible Substrates," *ACS applied materials & interfaces,* vol. 10, no. 4, pp. 3830-3837, 2018.

[27] J. Lefebvre, J. Ding, Z. Li, P. Finnie, G. Lopinski, and P. R. Malenfant, "High-purity semiconducting single-walled carbon nanotubes: a key enabling material in emerging electronics," *Accounts of chemical research,* vol. 50, no. 10, pp. 2479-2486, 2017.

[28] M. Ha *et al.*, "Printed, sub-3V digital circuits on plastic from aqueous carbon nanotube inks," *ACS nano,* vol. 4, no. 8, pp. 4388-4395, 2010.

[29] K. Hong *et al.*, "Aerosol Jet Printed, Sub‐2 V Complementary Circuits Constructed from P‐and N‐Type Electrolyte Gated Transistors," *Advanced Materials,* vol. 26, no. 41, pp. 7032-7037, 2014.

[30] L. Cai, S. Zhang, J. Miao, Z. Yu, and C. Wang, "Fully printed stretchable thin-film transistors and integrated logic circuits," *ACS nano,* vol. 10, no. 12, pp. 11459-11468, 2016.

[31] C. Cao, J. B. Andrews, and A. D. Franklin, "Completely Printed, Flexible, Stable, and Hysteresis‐Free Carbon Nanotube Thin‐Film Transistors via Aerosol Jet Printing," *Advanced Electronic Materials,* vol. 3, no. 5, p. 1700057, 2017.

[32] X. Cao, F. Wu, C. Lau, Y. Liu, Q. Liu, and C. Zhou, "Top-Contact Self-Aligned Printing for High-Performance Carbon Nanotube Thin-Film Transistors with Sub-Micron Channel Length," *ACS nano,* vol. 11, no. 2, pp. 2008-2014, 2017.

[33] B. Kim, M. L. Geier, M. C. Hersam, and A. Dodabalapur, "Inkjet printed circuits on flexible and rigid substrates based on ambipolar carbon nanotubes with high operational stability," *ACS applied materials & interfaces,* vol. 7, no. 50, pp. 27654-27660, 2015.

[34] H. Li, Y. Tang, W. Guo, H. Liu, L. Zhou, and N. Smolinski, "Polyfluorinated electrolyte for fully printed carbon nanotube electronics," *Advanced Functional Materials,* vol. 26, no. 38, pp. 6914-6920, 2016.

[35] J. Liang, K. Tong, and Q. Pei, "A water‐based silver‐nanowire screen‐print ink for the fabrication of stretchable conductors and wearable thin‐film transistors," *Advanced Materials,* vol. 28, no. 28, pp. 5986-5996, 2016.

[36] C. M. Homenick *et al.*, "Fully printed and encapsulated SWCNT-based thin film transistors via a combination of R2R gravure and inkjet printing," *ACS applied materials & interfaces,* vol. 8, no. 41, pp. 27900-27910, 2016.

[37] W. Lee *et al.*, "A fully roll-to-roll gravure-printed carbon nanotube-based active matrix for multi-touch sensors," *Scientific reports,* vol. 5, p. 17707, 2015.

[38] J. A. Cardenas, M. J. Catenacci, J. B. Andrews, N. X. Williams, B. J. Wiley, and A. D. Franklin, "In-Place Printing of Carbon Nanotube Transistors at Low Temperature," *ACS Applied Nano Materials,* vol. 1, no. 4, pp. 1863-1869, 2018.

[39] K. Hong, S. H. Kim, A. Mahajan, and C. D. Frisbie, "Aerosol Jet Printed p-and n-type Electrolyte-Gated Transistors with a Variety of Electrode Materials: Exploring Practical Routes to Printed Electronics," *ACS applied materials & interfaces,* vol. 6, no. 21, pp. 18704-18711, 2014.

[40] P. H. Lau *et al.*, "Fully printed, high performance carbon nanotube thin-film transistors on flexible substrates," *Nano letters,* vol. 13, no. 8, pp. 3864-3869, 2013.

[41] L. Cai, S. Zhang, J. Miao, Z. Yu, and C. Wang, "Fully printed foldable integrated logic gates with tunable performance using semiconducting carbon nanotubes," *Advanced Functional Materials,* vol. 25, no. 35, pp. 5698-5705, 2015.

[42] J. Lefebvre, J. Ding, Z. Li, F. Cheng, N. Du, and P. Malenfant, "Hysteresis free carbon nanotube thin film transistors comprising hydrophobic dielectrics," *Applied Physics Letters,* vol. 107, no. 24, p. 112_1, 2015.

[43] P. Chen *et al.*, "Fully printed separated carbon nanotube thin film transistor circuits and its application in organic light emitting diode control," *Nano letters,* vol. 11, no. 12, pp. 5301-5308, 2011.

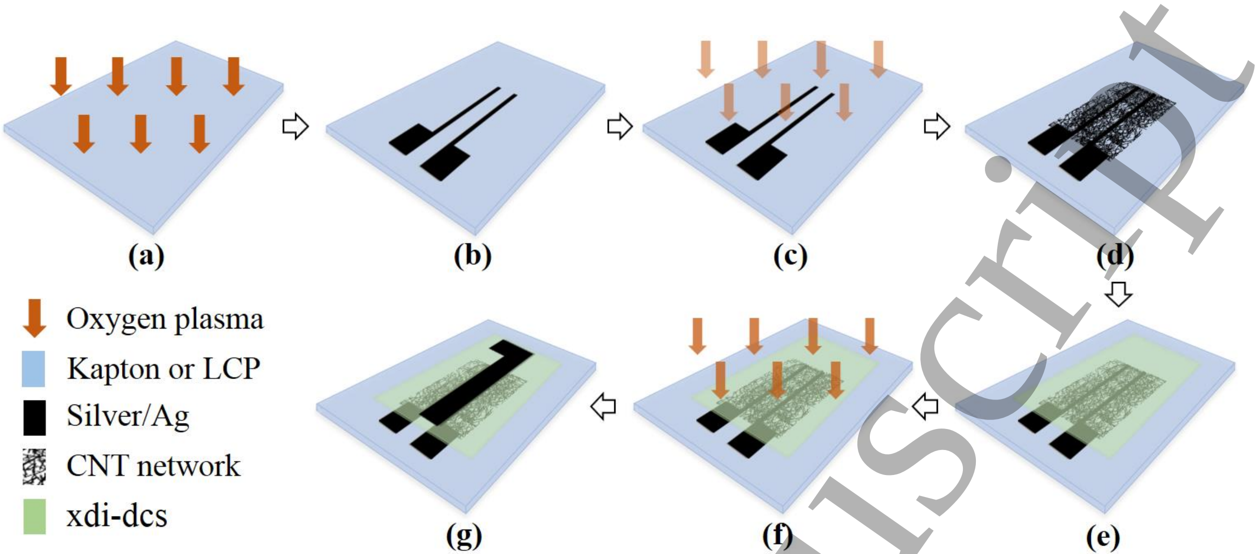

Figure 1. Schematic of the fabrication process of fully printed CNT-TFTs on flexible substrates using AJP. (a) A well prepared flexible substrate (either Kapton or LCP) which is cleaned by 3-5min oxygen plasma before printing. (b) Ag printing to fabricate S/D electrodes. (c) 1min oxygen plasma treatment before CNT printing for better wetting. (d) CNT network printing using a multiple layer by layer printing method. (e) Dielectric layer/xdi-dcs printing. (f) 2-3min oxygen plasma treatment before Ag printing. (g) Ag printing as a top gate electrode. A fully printed CNT-TFT is fabricated following these steps. Note: Ag is cured at 150°C for 15~25min. Dielectric layer/xdi-dcs is cured at 140°C for 20min.

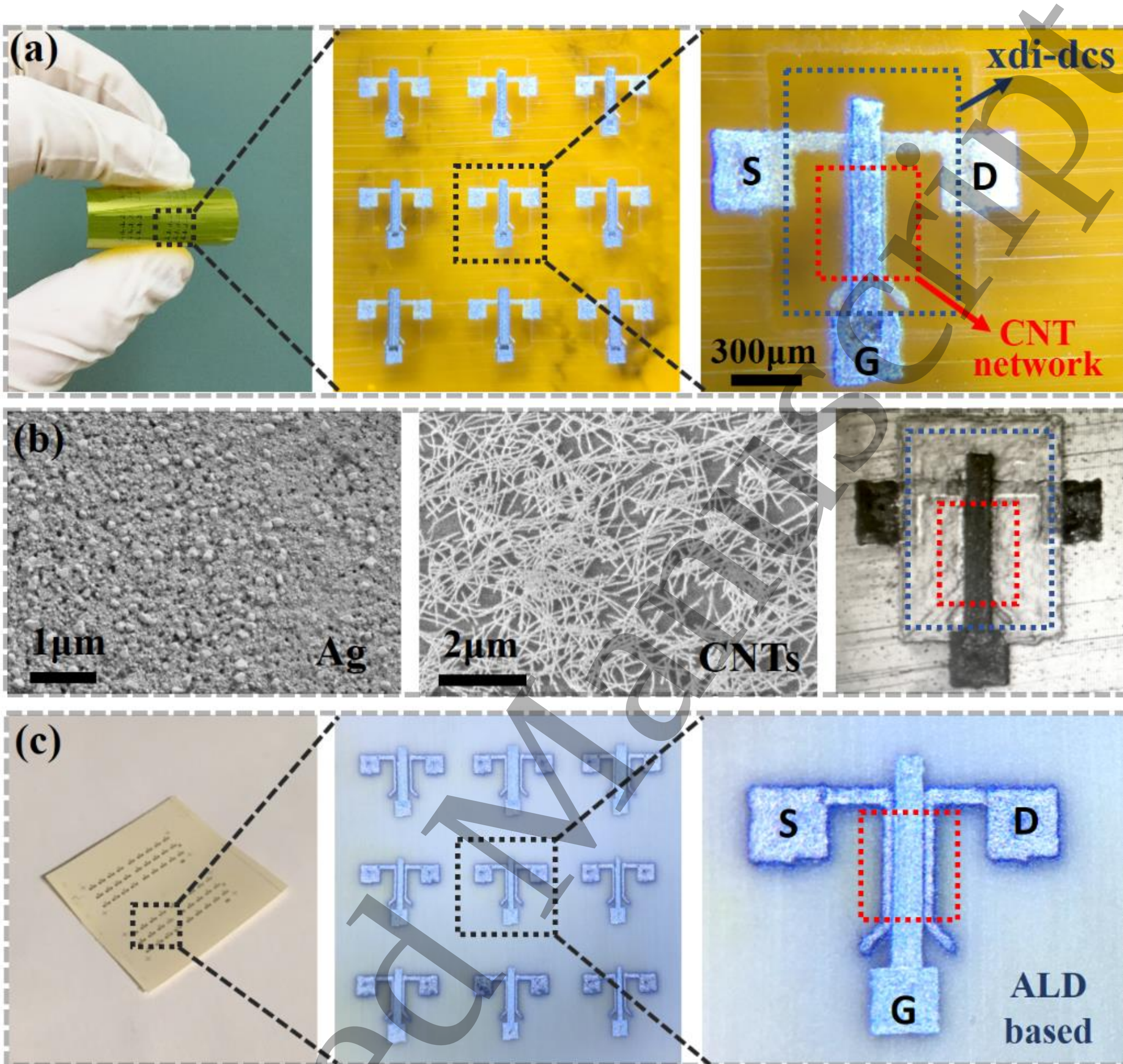

Figure 2. Features and morphology of printed CNT-TFTs. (a) Fully printed CNT-TFTs on Kapton substrate using xdi-dcs dielectric layer. xdi-dcs layer is a transparent thin film under microscope where CNT network (denoted by red dash box) is almost invisible in the channel. (b) SEM images show morphology of Ag electrodes, CNT network, and a CNT-TFT. (c) Printed CNT-TFTs on LCP substrate using ALD dielectric layer.

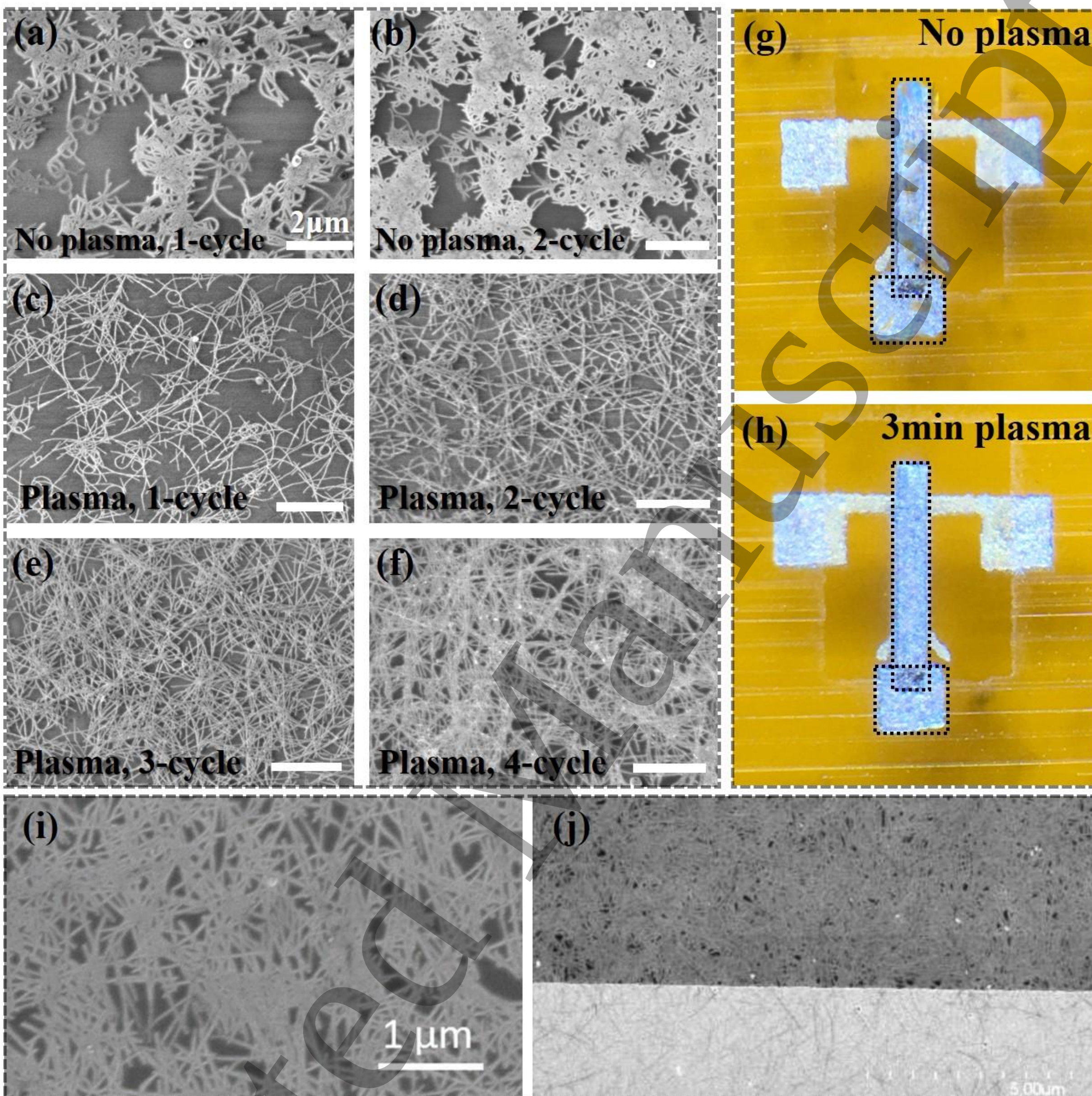

Figure 3. The effects of oxygen plasma treatment before CNT network printing (a)-(f) and Ag printing (g)-(h) on top of xdi-dcs thin film. Without plasma treatment, CNTs bundle together easily (a)-(b) and Ag thin film is uneven with huge pinholes everywhere (g). CNT network density can be well controlled by layer-by-layer deposition after plasma treatment (c)-(f). Scale bar is 2μm in (a)-(f). (i) and (j) are the SEM images from [31] and [36] respectively, the densities of which are much higher than in (c)-(d). The improvement in printing conductive single layer of CNT network (very low density) results in the increase of on/off ratio of the fully printed CNT-TFTs.

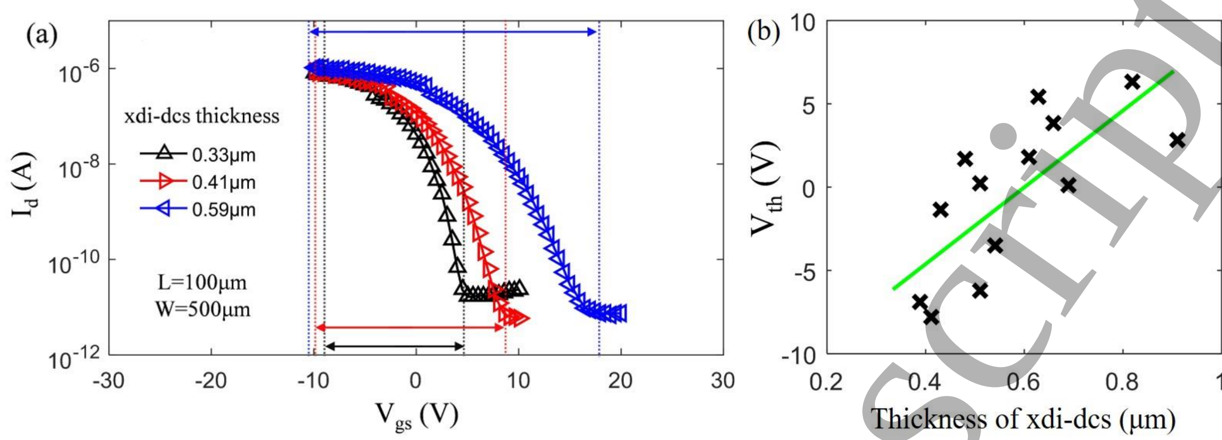

Figure 4. The impact of the printed xdi-dcs layer on the performance of fully printed CNT-TFTs. (a) Comparison of transfer curves of three fully printed CNT-TFTs with different thickness of dielectric layers. (b) The dependence of V_{th} on the thickness of printed xdi-dcs thin films for fully printed CNT-TFTs.

Table 1. Performance comparison and fabrication details of printed CNT-TFTs in literature. Generally, ALD based device has better performance and stability, but the cost is high. Ion-gel based devices can achieve low operation voltage, but it is physically fragile. This work achieved better performance for fully printed flexible devices using xdi-dcs as dielectric based on single printing method (In Ref. [36], fabricated devices are not based on a single printing method and most of the data is for devices fabricated on hard substrate). The reference with stars (*[33], *[42], and *[36]) denotes the usage of an encapsulation layer for the back-gated devices.

Reference	**Operation voltage V_g**	**Hysteresis**	**Best On/off ratio**	**Fully printed**	**Dielectric**	**Fabrication**
*[33]	~4V	~0.6V	~10^4	No	ALD based	IJP/Photolithography
[40]	~6V	~3.8V	>10^5	Yes	ion-gel	Gravure with masks
[28]	~1.5V	~0.4V	>10^5	No	ion-gel	AJP/Photolithography
[43]	~1V	~0.1V	N/A	Yes	ion-gel	IJP
[41]	~20V	~5V	<10^4	Yes	$BaTiO_3$/PMMA	IJP-like
[30]	~30V	~4V	<10^4	Yes	$BaTiO_3$/PMMA	Printing with masks
*[42]	~15V	~0.03-0.45V	~10^4	No	xdi-dcs, Teflon-AF	Spin coat/AJP based
[31]	~40V	~0.5V	~10^5	Yes	xdi-dcs	AJP
*[36]	~5V	~0.2V	>10^4	Yes	$BaTiO_3$	IJP/R2R
This work	~6V	~0.6V	>10^5	Yes	xdi-dcs	AJP

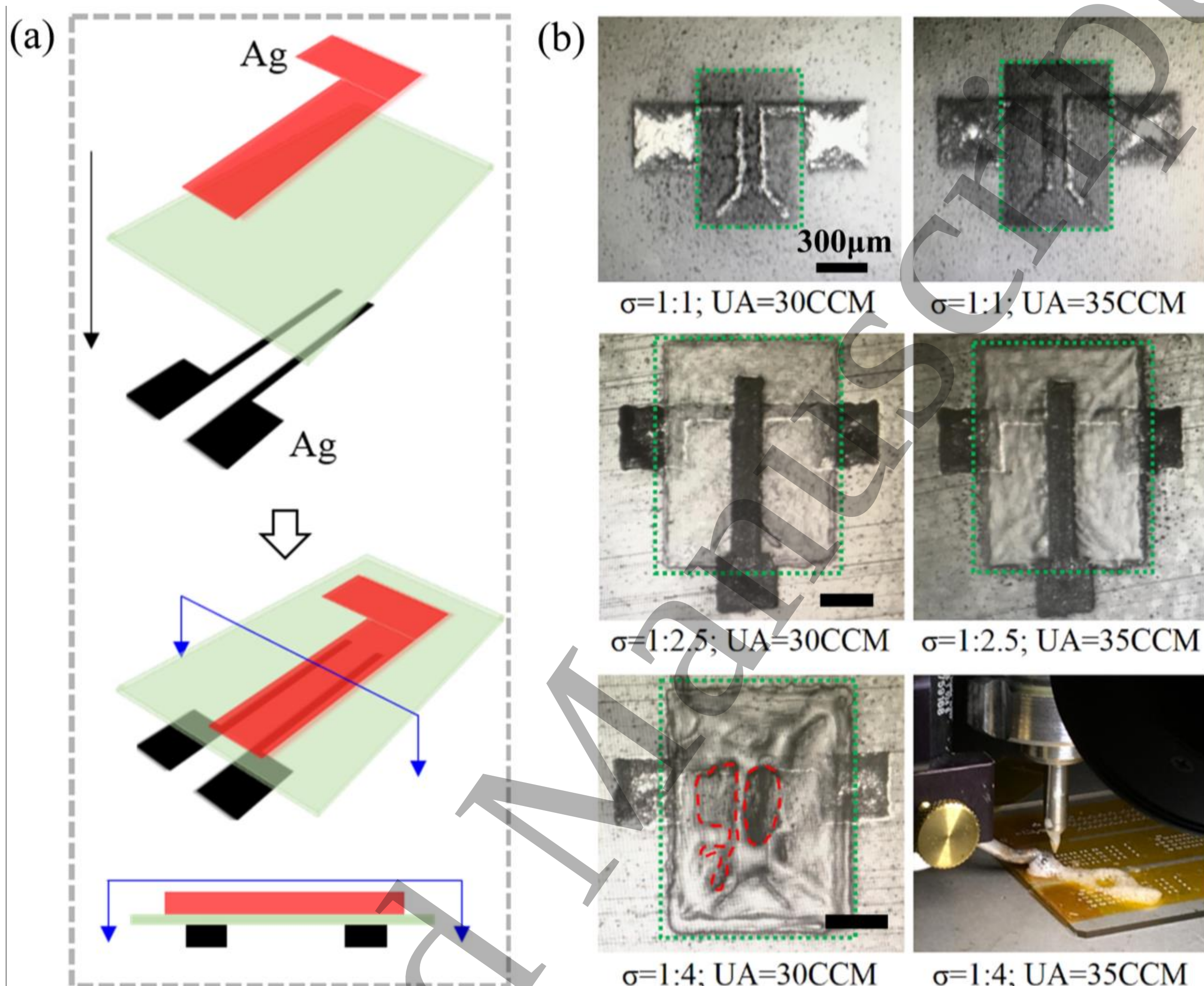

Figure 5. (a) Schematic structure (layer-by-layer structure and the sectional view) used to test the insulation quality of printed xdi-dcs thin films (light green layer). (b) Visualization of printed xdi-dcs thin film at different dilute ratio σ (1:1, 1:2.5, and 1:4) and ultrasonic atomizer flow rate UA (30CCM and 35CCM). The thin films in upper figures will not work well for devices as numerous pinholes are present because of the particle-like behavior during xdi-dcs printing. That means the concentration of dielectric ink is still too high since σ is only 1:1. The middle figures show well printed xdi-dcs thin films. No pinholes exist when σ is 1:2.5 and the thickness of printed dielectric layers can be controlled by UA. The thin films in lower figures will not work either because of the over printing, which can result in several big pinholes (denoted by red dash area, left) and even ruin the substrate (right). That means the concentration of dielectric ink is still too low when σ is 1:4. All scale bars are 300μm.

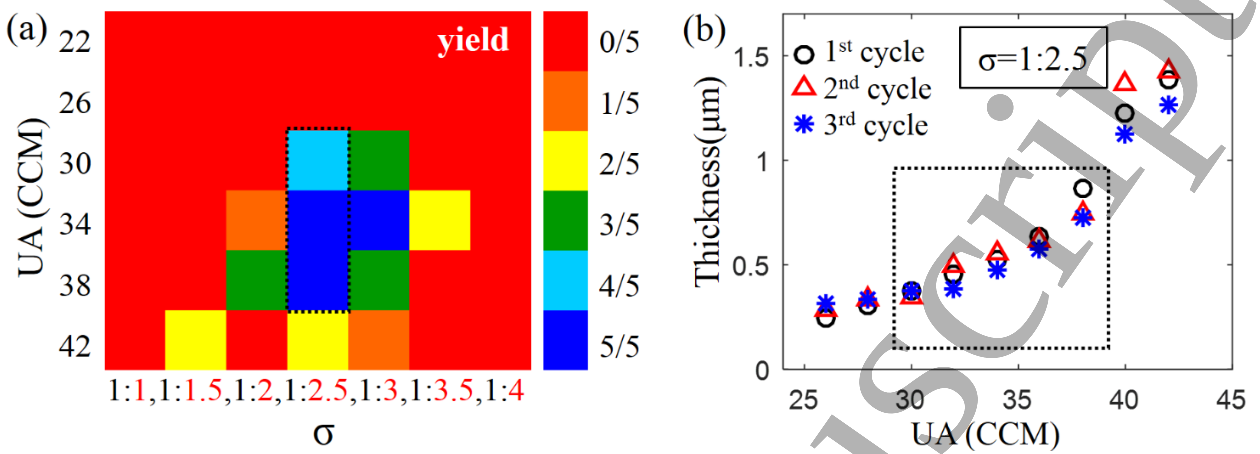

Figure 6. Optimization of printed xdi-dcs thin film. (a) Yield rate (number of samples with good insulation quality which has leakage current much less than off current of the corresponding transistors ~0.1nA) under different σ and UA combinations. (b) Thickness dependence of xdi-dcs thin film on UA when σ equals to 1:2.5, which is the best σ from (a). The black dash box in (a) and (b) denotes UA range of 30-38CCM at best σ.

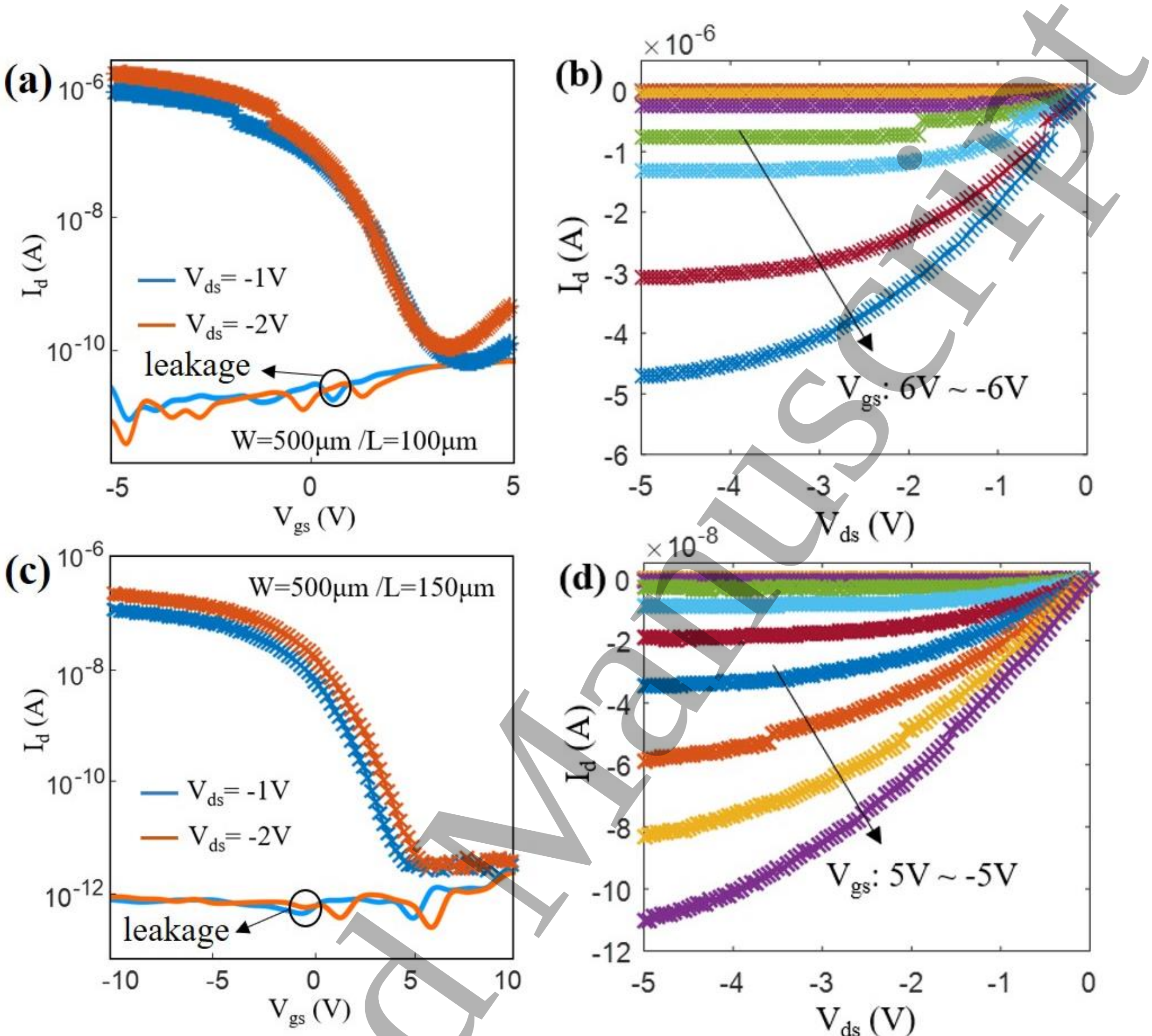

Figure 7. I-V characteristics of CNT-TFTs. Transfer curve (a) and output curve (b) of an ALD based printed CNT-TFTs (~80nm Al_2O_3, W=500µm, L=100µm, 1-cycle CNT network deposition). Transfer curve (c) and output curve (d) of a fully printed CNT-TFTs based on printed dielectric layer with thickness as small as 0.3µm (W=500µm, L=150µm, 3-cycle of CNT network deposition).